Supplementary Information

● Memristive feature and mechanism induced by laser-doping in defect-free 2D semiconductor materials

Xiaoshan Du‡[1,2], Shu Wang‡[2], Qiaoxuan Zhang‡[3], Shengyao Chen‡[2,4], Fengyou Yang[2], Zhenzhou Liu[2], Zhengwei Fan[2], Lijun Ma[2], Lei Wang[5], Lena Du[6], Zhongchang Wang[7], Cong Wang†[8], Bing Chen†[1] and Qian Liu†[2,4]

[1]College of Electronic and Information Engineering, Shandong University of Science and Technology, Qingdao, 266590, Shandong, China

[2]National Center for Nanoscience and Technology & University of Chinese Academy of Sciences, Beijing 100190, China

[3]Hebei University of Water Resources and Electric Engineering Electrical Automation Department, 061001 Cangzhou, Hebei, China

[4]The MOE Key Laboratory of Weak-Light Nonlinear Photonics and International Sino-Slovenian Join Re-search Center on Liquid Crystal Photonics, TEDA Institute of Applied Physics and School of Physics, Nankai University, Tianjin 300457, China

[5]College of Mathematics and Physics, Shandong Advanced Optoelectronic Materials and Technologies Engineering Laboratory, Qingdao University of Science and Technology, Qingdao, 266061, China

[6]Department of Physics, Capital Normal University, Beijing 100048, China

[7]Department of Advanced Materials and Computing, International Iberian Nanotechnology Laboratory (INL), 4715-330 Braga, Portugal

[8]College of Mathematics and Physics, Beijing University of Chemical Technology, Beijing 100029, China

Xiaoshan Du, Shu Wang, Qiaoxuan Zhang, and Shengyao Chen contributed equally to this work and should be considered as co-first authors.

Corresponding authors:
wangcongphysics@mail.buct.edu.cn,
chenbing@sdust.edu.cn,
liuq@nanoctr.cn

Section S1. Device preparation process and device characterisation

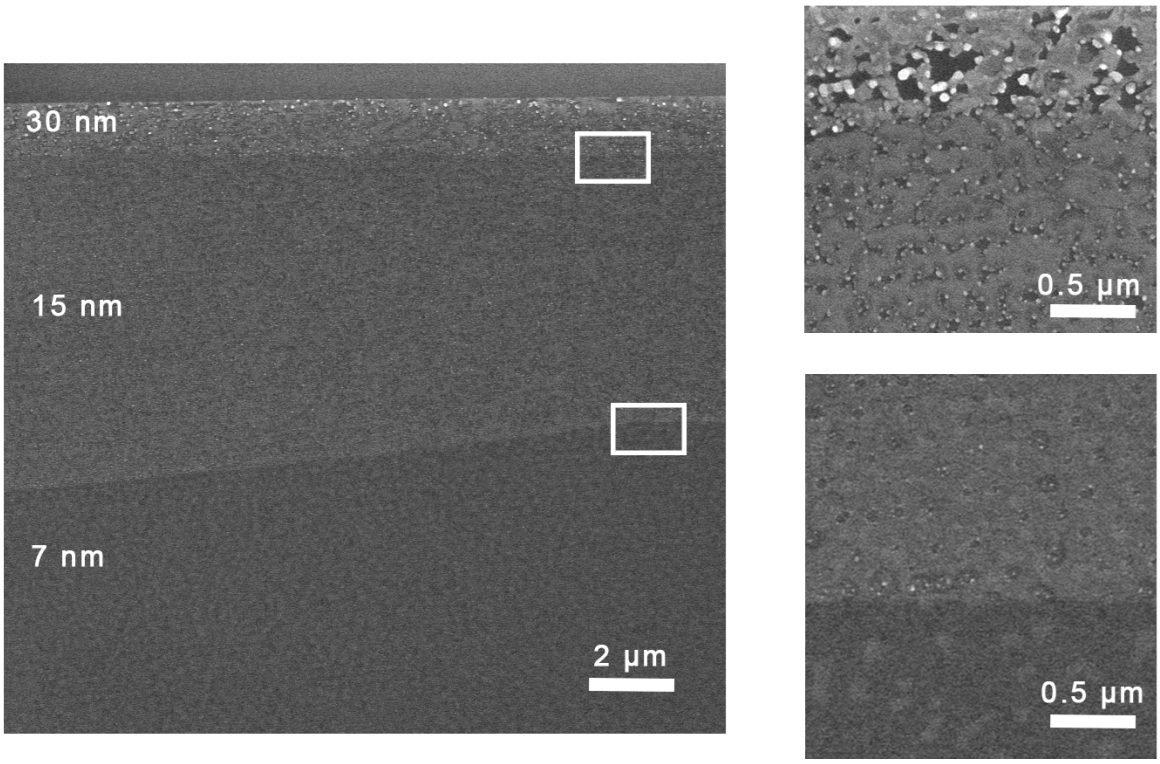

Fig. S1. SEM images of the same power density (280 KW·mm^{-2}) laser on MoS_2 with different thicknesses (30 nm, 15nm, 7 nm).

Thinner materials tend to require higher power due to low heat capacity, and thicker materials tend to have an effect on laser parameters due to excessive heat capacity. we use the same power density (280 KW·mm^{-2}) on different thicknesses of the material, the thicker material due to the absorption of more energy, the greater degree of destruction.

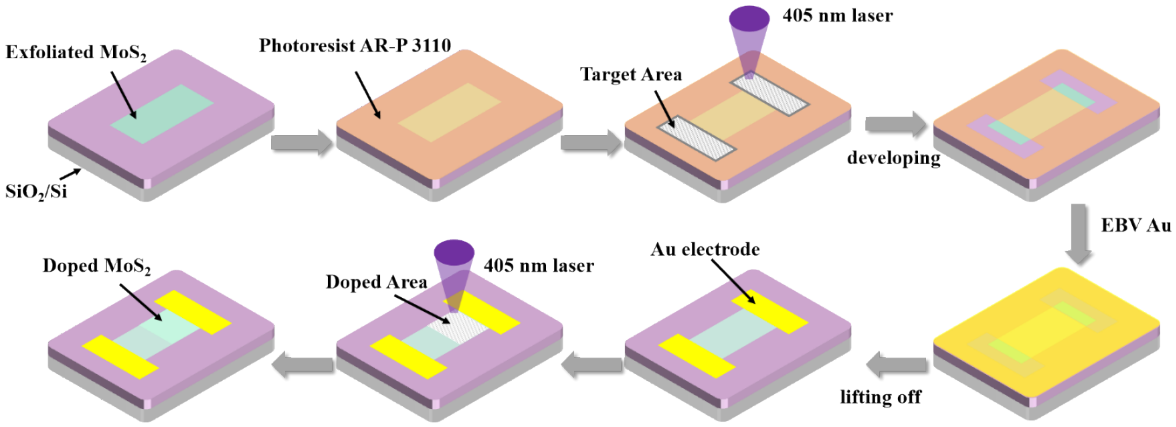

Fig. S2. Schematic diagram of the device preparation process.

The experiment involves the selection of few-layers MoS_2 prepared by mechanical exfoliation and Si/SiO_2 substrate. The electrode is prepared through laser direct writing lithography, using AR-P 3110 positive photoresist. The resist spin-coating is performed at a speed of 3000 RPM for 60 s, followed by baking at 120°C for 90 s to evaporate the solvent. After spin-coating, the resist is exposed using a maskless lithography system (LDW, HWN-LDW-L4) with laser parameters of 0.3 mW power and 2000 ns pulse width. The development process takes about 90 s. The metal top electrode is prepared using e-beam evaporation, and the resist is removed using acetone. Finally, laser direct writing is used to complete the doping process.

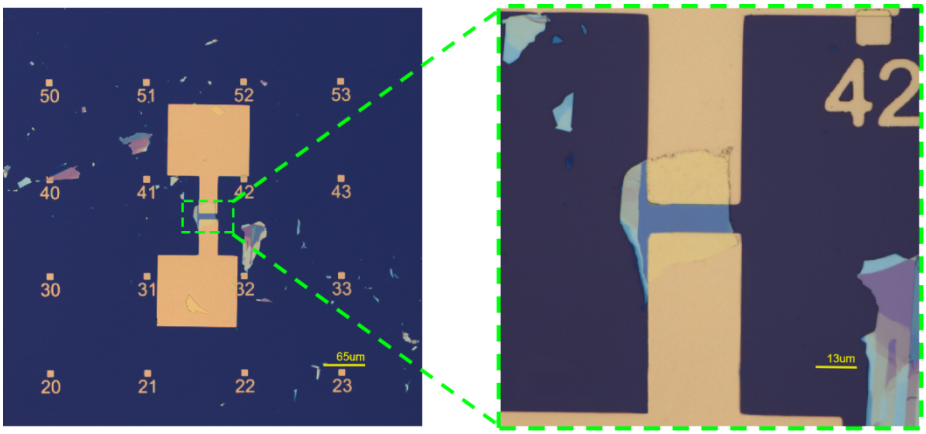

Fig. S3. Optical microscope scan of the physical image of the device (20×) and a magnified detail image (50×).

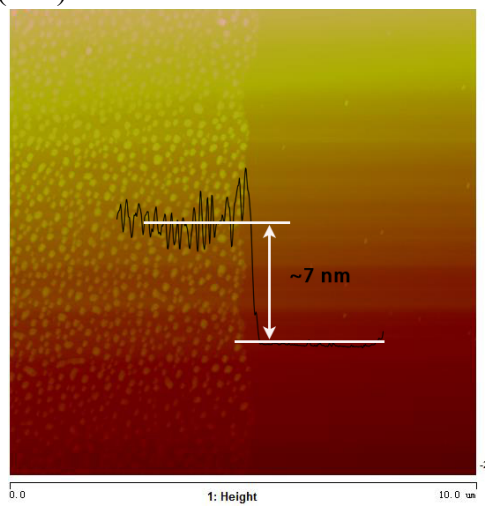

Fig. S4 AFM image of MoS_2 used in the preparation of the device. AFM result shows that the experimental material thickness is about 7 nm.

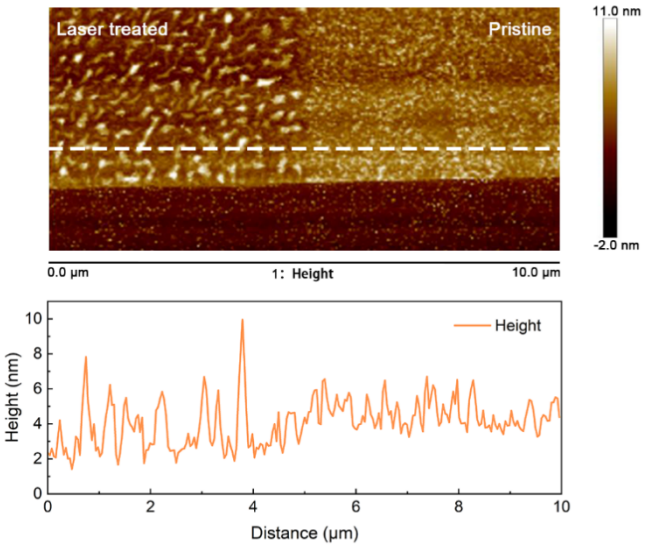

Fig. S5 AFM image of MoS_2 after 280 KW • mm^{-2} laser actionused in the preparation of the device. AFM result shows that the surface of the material is visibly changed by the laser action.

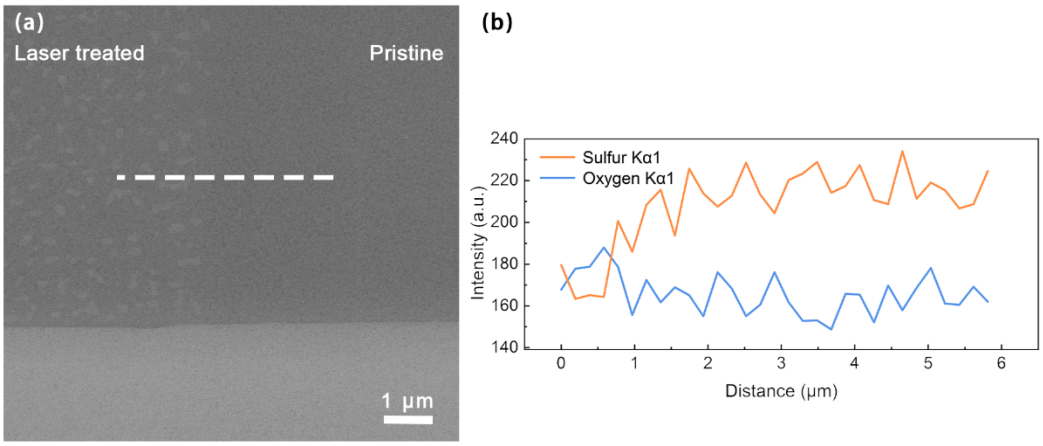

Fig. S6 (a) Laser treated and pristine MoS_2 SEM images. **(b)** EDS line scanning elemental analysis results, showing an increase in O and a corresponding decrease in S after laser action.

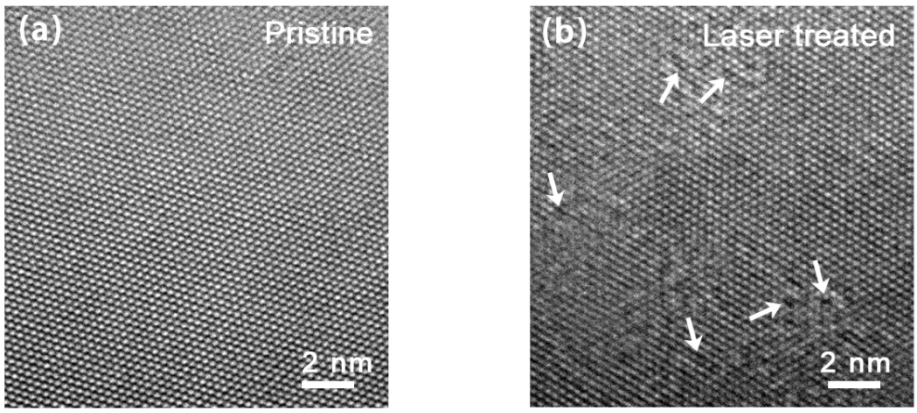

Fig. S7 (a) HRTEM image of pristine MoS_2. (b**)** HRTEM image of laser treated MoS_2.

From the high resolution transmission electron microscope (HRTEM) images, it is obvious that the intrinsic MoS_2 is structurally complete with an orderly lattice arrangement, whereas the lattice integrity and order are obviously destroyed after being subjected to laser action. This is due to the fact that the M−O bond strength is higher than the M−S bond, which leads to the shift of the particle position.[1]

Section S2 Simulation Calculation

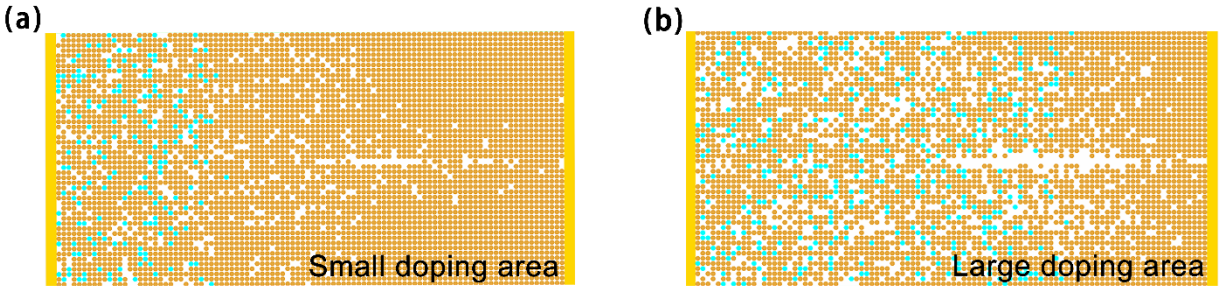

Fig. S8. (a) Monte Carlo simulation results after laser doping of 1/3 region. **(b)** Monte Carlo simulation results after laser doping of 2/3 region.

Fig. S8(a) shows the migration behavior within the device system when the doped region occupies only 25% of the device. Although the vacancy density and low doping conditions are similar, the prolonged migration process in the device leads to a more pronounced tip discharge effect. Additionally, devices with smaller doped regions have higher initial resistance, resulting in some improvement in terms of opening and low doping concentration compared to the devices. **Fig. S8(b)** demonstrates the migration behavior of devices with an increased doped region. It can be observed that the device

forms well-defined conducting filaments. However, due to the lower initial resistance of this device, it exhibits a smaller opening compared to devices with low doping concentrations.

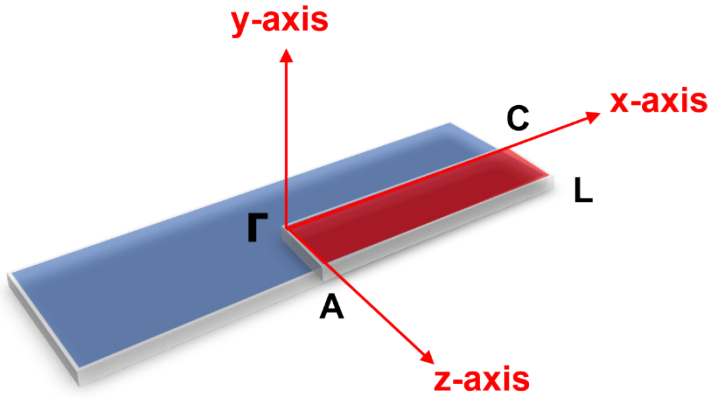

Fig. S9. The brillouin zone scanning path of the bands is Γ−A−L−C−Γ

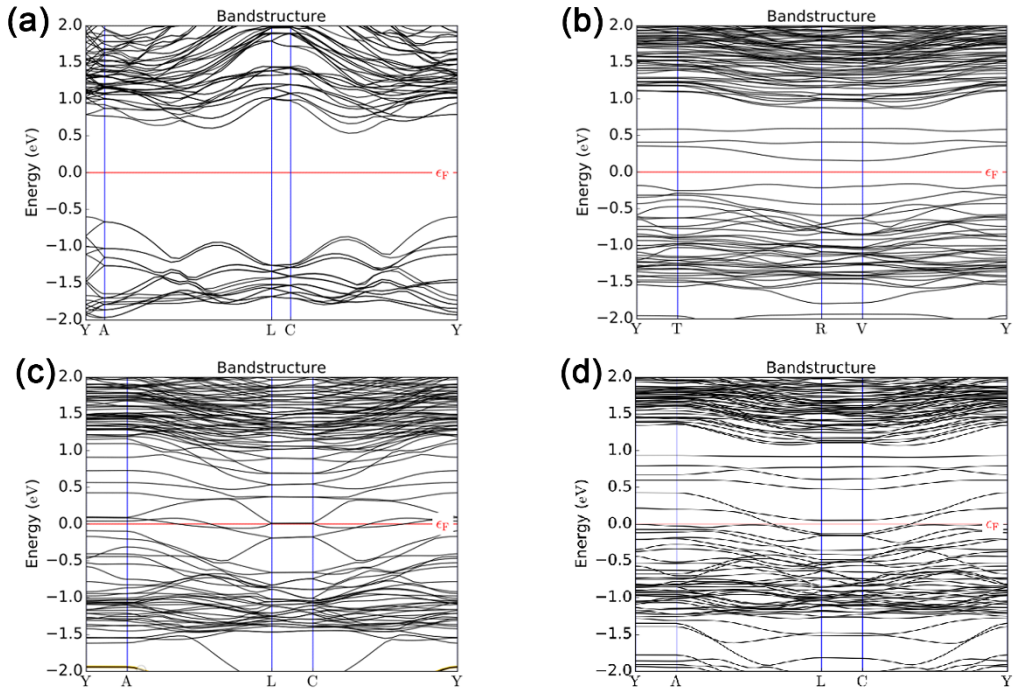

Fig. S10. (a) Pristine MoS_2. The indirect band gap is 1.14 eV. **(b)** MoS_2 with one S vacancy and one oxygen substitution on the right half-plane. The indirect band gap is 0.32 eV. **(c)** MoS_2 with two S vacancies and two oxygen substitutions on the right half-plane and **(d)** fully doped MoS_2 is metal.

The bands and LDOSs are conducted by Quantum Atomistic ToolKit (ATK) ver. 2019[2]. The electronic properties of the atoms are calculated by local-density approximation DFT-1/2 method according to non-equilibrium Green's function (NEGF).[3, 4] The overall structure is cut from bilayer 1×1 MoS_2 unit cells (lattice

parameter atheo=3.30 Å，ctheo=13.10 Å). All the structures are optimized by ATK. The k-point meshes 32×1×4 are used to optimize the a and d geometric structures,[5] 16×1×4 for b and c. The stress force and energy convergence criteria are chosen as 0.01 eV/Å [6] and 10^{-5} eV, respectively. The exchange correlation type is LDA-1/2 with PZ predefined functionals and Dirac Bloch exchange corrected by Perdew-Zunger self-interaction correlation. [7] FHI pseudopotential with Double ζ polarized (DZP) basis sets are adopted for all atoms. The inner electrons are described Real-space grids are set to 75 Hartree and the simulation temperature is set to 300 K. The convergence criterion of the Hamiltonian is 1×10^{-4} Hartree, and after reaching the convergence, 32×1×100 k points are sampled for a,d and 16×1×100 k points for b,c to calculate LDOSs.

Section S3 Influence of laser power on doping level

Table S1. Laser doping concentration results.

Elements / **Percentage (%)** / **Laser power**	Oxygen	Sulfur	Molybdenum	$\frac{\text{Oxygen}}{\text{Molybdenum}}$
0 mW	11.81	57.6	30.58	0.38
8.21 mW	12.09	57.4	30.44	0.40
11.1 mW	14.3	55.15	30.55	0.46
19.8 mW	21.19	47.23	31.58	0.67

Section S4. Laser interaction with MoS_2

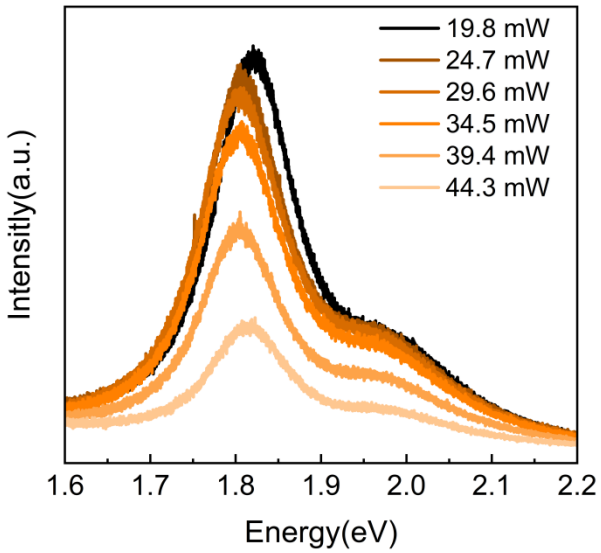

Fig. S11. PL spectra of MoS_2 at laser powers above 19.8 mW.

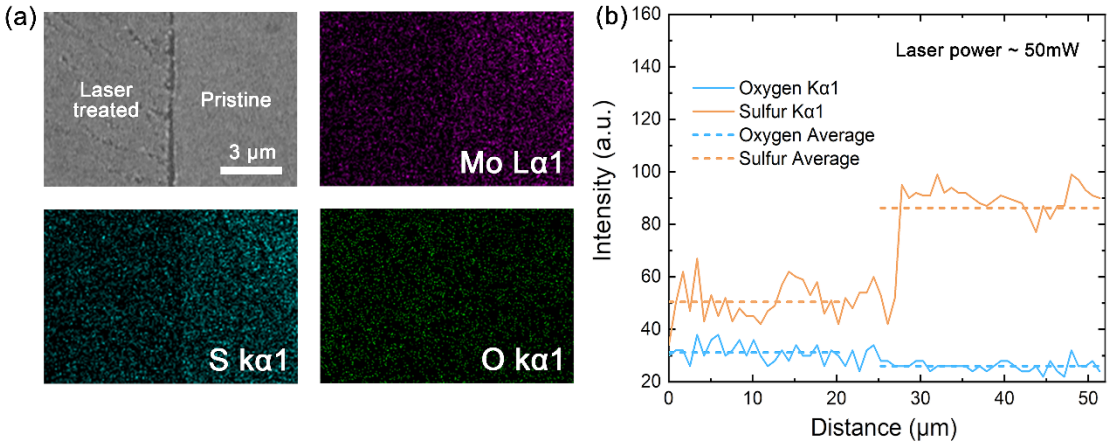

Fig. S12. (a) Laser treated and pristine MoS_2 SEM images with EDS elemental analysis results. **(b)** EDS line scanning elemental analysis results.

In order to further confirm the changes in MoS_2 after laser treatment, we performed compositional analysis on the laser-treated MoS_2 using an energy-dispersive spectrometer (EDS). The scanning electron microscopy (SEM) image and EDS elemental surface distribution results are shown in **Fig.S12(a)**. We selected the MoS_2 in the laser-treated area with a power of 50 mW (maximum power) and the untreated area for characterization. We found that the laser-treated area exhibited obvious cracks and thinning in morphology. Elemental distribution analysis showed a significant decrease in both molybdenum and sulfur elements in the laser-treated area, while there was no apparent regularity in oxygen elements. We plotted the changes in oxygen and sulfur elements as a function of lateral distance, as shown in **Fig. S12(b)**. It can be observed from the figure that after laser treatment, the distribution of oxygen elements only slightly increased, but the sulfur content decreased significantly. This result further confirms that excessive laser power can damage the material's structure.

References

[1] Zhu H, Jin R, Chang Y C, et al. Understanding the Synergistic Oxidation in Dichalcogenides through Electrochemiluminescence Blinking at Millisecond Resolution. Adv Mater, 2021, 33: 10

[2] ToolKit A CP/OL. QuantumWise, http:// www. quantumwise. com, 2014,

[3] Ferreira L G, Marques M and Teles L K Approximation to density functional theory for the calculation of band gaps of semiconductors. Phys Rev B, 2008, 78: 125116

[4] Brandbyge M, Mozos J-L, Ordejón P, et al. Density-functional method for nonequilibrium electron transport. Phys Rev B, 2002, 65: 165401

[5] Chadi D J and Cohen M L Special points in the Brillouin zone. Phys Rev B, 1973, 8: 5747

[6] Monkhorst H J and Pack J D Special points for Brillouin-zone integrations. Phys Rev B, 1976, 13: 5188

[7] Vydrov O A and Scuseria G E Ionization potentials and electron affinities in the Perdew–Zunger self-interaction corrected density-functional theory. J Chem Phys, 2005, 122: